APPLICATION OF THE METHOD OF OPTIMISED IMAGES TO STEADY THREE-DIMENSIONAL CONDUCTION PROBLEMS

K.J. Negus* and M.M. Yovanovich†

Thermal Engineering Group
Department of Mechanical Engineering
University of Waterloo
Waterloo, Ontario

ABSTRACT

The analytical/numerical method of optimised images is presented in terms of steady three-dimensional heat conduction. This novel technique which can solve field problems from several engineering disciplines is particularly useful for difficult flux tube problems in contact resistance. The methodology and implications of the optimised image technique are examined in detail for the concentric circular flux tube with uniform contact flux. To find the thermal constriction resistance for this problem, the temperature fields due to a circular contact and one to three circular ring source images on a half-space are superposed in some "optimal" combination such that the physical boundary conditions for the flux tube are best approximated. In addition by solving for the constriction resistance of a circular contact on a square flux tube with two different contact flux distributions, the potential power of the method of optimised images in steady heat conduction is demonstrated.

Since the latter results are useful for ongoing research in contact resistance, simple but accurate correlations of the dimensionless constriction resistance parameter are provided for a large range of relative contact sizes.

NOMENCLATURE

a	- circular contact radius
A_t	- cross-sectional area of flux tube
A_{2n}	- series coefficients
b	- radius of circular flux tube, half-width of square flux tube
$C^{3/2}_{2n-3}(\cdot)$	- Gegenbauer polynomial of order 2n-3
e_j	- residual boundary-flux at test-point
$E(\cdot)$	- complete elliptic integral of second kind
E_t	- sum of residual boundary-fluxes squared
$J_1(\cdot)$	- Bessel function of order 1
k	- thermal conductivity
$K(\cdot)$	- complete elliptic integral of first kind
ℓ	- half-length of finite-line source image
L	- depth at which average temperature in a flux tube cross-section is calculated
M	- number of optimised images
N	- number of test-points
NR	- number of optimised circular ring images
$P_{2n-2}(\cdot)$	- Legendre polynomial of order 2n-2
q	- flux distribution over contact area
q_o	- uniform flux over contact area
q^c_j	- flux at test-point due to circular contact
Q^c	- total heat flux over circular contact
Q, Q_i	- line strength of circular ring and finite-line sources
r	- spherical coordinate
R, R_i	- radius of circular ring source image
R_c	- thermal constriction resistance
R_m	- material resistance
T	- temperature rise
$\overline{T}_c$	- average temperature rise on contact
$\overline{T}(z=L)$	- average temperature rise on flux tube plane z=L
x,y,z	- Cartesian coordinates
x_o, y_o	- distance between finite-line sources and axes

Greek symbols

α	- ratio of flux tube length to radius
δ_n	- eigenvalue solutions of $J_1(\delta_n) = 0$
ε	- dimensionless contact size, a/b
θ	- spherical coordinate
λ	- modulus of complete elliptic integrals
ρ	- polar coordinate
σ,τ,β	- parameters used in expressions for temperature rises and fluxes
ϕ_j	- relative residual-boundary flux

* Research Assistant
† Professor, Member ASME

ψ - thermal constriction resistance parameter, $4kaR_c$

Subscripts

i - refers to an optimised image

j - refers to a test-point

INTRODUCTION

In this work the method of optimised images will be demonstrated by solving steady, three-dimensional, thermal constriction resistance flux tube problems. A thermal constriction resistance flux tube consists of a finite contact area located on the top surface of a semi-infinite rod of constant cross-sectional shape. Both the sides of the rod and the top surface excluding the contact area are adiabatic. Heat is supplied through the finite contact area and flows down the length of the rod to a sink at infinity.

In most contact resistance problems, both the contact shape and the flux tube cross-sectional shape are usually modelled as circles, ellipses, squares or rectangles. This modelling is made for two reasons. First the theory describing the mechanical interaction between two rough surfaces is not sufficient to predict the exact actual shape of any given contact. And second because of the statistical nature of the analysis which deals with the vast numbers of microcontacts, only the "average" or "typical" unit cell need be considered to give adequate results. For example in the classical theory of conforming rough surfaces [1], the flux tube geometry is usually a circular contact on a concentric circular flux tube, or perhaps more correctly, a circular contact on a concentric square flux tube. The circular flux tube is illustrated in Fig. 1. In the study of cylinder-flat contacts [2], McGee found elliptical contacts forming on rectangular flux tubes. And in the proposed work of DeVaal [3], anisotropic roughness between conforming surfaces should create non-concentric elliptical contacts on elliptical flux tubes. Solution to these complex three-dimensional heat flow problems is extremely difficult by purely analytical techniques and usually computationally time-consuming by fully numerical techniques. In addition for most problems of interest in contact resistance, the contact area is much smaller than the cross-sectional area of the flux tube. For this geometry the single-infinite and double-infinite series summations of the analytical solutions require many thousands of terms. However as will be seen in the results which follow, the method of optimised images has a maximum efficiency for solution which corresponds to this case of small contact area. Thus one major motivation for developing the optimised images technique in heat conduction is the potential ability to solve more efficiently several complex but practical problems in contact resistance. Another motivation for this analytical/numerical technique is its ability to solve flux tube problems where solution was previously possible only by fully numerical methods such as finite difference or finite elements. One excellent example of this from practical contact resistance problems is the constriction resistance of an elliptical contact area located off-center in an elliptical or rectangular flux tube [2,3]. Finally, the method of optimised images can also find application in other thermal conduction problems as well as electrostatic capacitance problems and ideal fluid flow problems.

The usual boundary condition for the top of the flux tube is an isothermal contact area and an adiabatic region over the remainder of the top of the flux tube. Although this creates a mixed boundary value problem, a solution was recently obtained [4] for a wide range of contact to flux tube size ratios for the circular contact on a circular flux tube. By comparing these results with those of the flux-specified contacts of Yovanovich [5], the uniform flux and equivalent isothermal flux provided respectively upper and lower bounds of the true isothermal constriction resistance over the entire range of contact to flux tube size ratios. The equivalent isothermal flux as used here is merely the flux distribution which results when an isothermal contact is placed on an adiabatic half-space.

In this work the validity of the optimised image approach will be confirmed by first considering in detail the problem of a concentric circular flux tube with uniform flux as described in [5]. In addition the potential power of the method will be demonstrated by solving the more complex problem of a circular contact on a square flux tube for both the uniform and equivalent isothermal flux cases.

The analytical method of solving field problems using images originated more than a century ago. The image method was particularly well suited for electrostatic problems where point or line charges were placed near grounded, insulated or dielectric surfaces or bodies. For many such problems, a single image point or line source could be easily located and the corresponding source strength simply calculated so that the physical boundary condition(s) could be met. For some more complex problems, examination of "rays" emanating from the original point or line charge would lead to an optical analogy for placing an infinite series of easily determined sources and/or sinks. The word "image" probably comes from this optical analogy.

The basic methodology for finding the field in one region consists of placing discrete images exterior to the region of interest such that all boundary conditions are satisfied. Then according to the uniqueness theorem [6,7,8], if all boundary

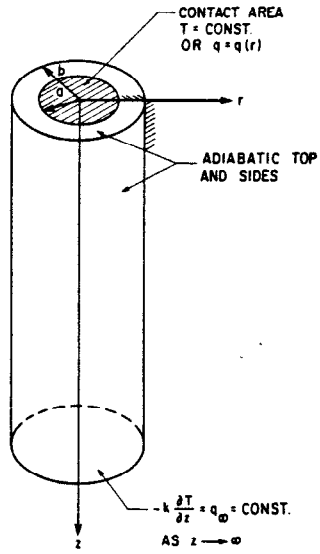

Fig. 1 Concentric circular flux tube

conditions are satisfied exactly and the images lie outside a given closed region, then when the solution so obtained by solving for the images is superposed with the original potential field without the images, the exact potential field within the given closed region results.

Several excellent examples of the analytical image technique are contained in Smythe [6]. Unfortunately, when the heat sources or boundaries become disks, spheres, prolates or some arbitrary shapes, determination of the correct image placements and strengths becomes an increasingly difficult (and usually non-linear) problem.

In 1979 Chow and Charalambous [9] published a paper on the use of "optimised simulated images" in electrostatic field problems. Their basic methodology was similar to the classical, analytical method of images except that they adopted the engineering approach that the boundary conditions need only be satisfied "approximately". As in the analytical method, the images were discrete sources or sinks, such as points or finite-lines, with variable size, strength and location. The boundary condition was then written such that the total sum of boundary residuals (usually squared) over a number of test points must be minimized. A boundary residual represents the difference between the approximate calculated boundary value and the exact boundary value desired. Unfortunately the relationship between the boundary residual sum and the image sizes and locations is non-linear. However, solution can be made using one of a variety of modern, computer-oriented, non-linear optimisation algorithms and Chow has had good success with the Fletcher algorithm [10]. In addition Chow, et. al. have demonstrated the validity of this technique in their type of problems by considering the variational bounds [11].

The problems which Chow has addressed generally require the images within conducting bodies exposed to an external field. In these problems the boundary conditions are Dirichlet specified by the isopotential requirements of the conducting bodies. The external "driving" field is outside the conducting bodies and thus the images, usually points or finite-lines, are located within the conducting bodies.

The approach of this work will be somewhat similar to that of Chow except for two major differences. First the formulations will be written in terms of heat conduction. Second the example problems have images located on the surface of a half-space external to the closed body of the flux tube.

CONSTRICTION RESISTANCE OF CONCENTRIC CIRCULAR FLUX TUBES BY OPTIMISED IMAGES

To gain experience with and investigate the potential power of the method of optimised iamges, a simple, well-understood problem with a useful closed form analytical solution was needed. The obvious choice from the topic of flux tubes is a concentric circular flux tube with a Neumann-specified circular contact. The analytical solution [5] consists of a single infinite summation of Bessel, rational and sine functions which converges typically with 500 to 2000 terms depending on the relative contact size. In particular, a uniform flux over the contact will be considered.

Formulation of Boundary Condition for Approximate Flux Tube

In Fig. 2 a circular contact on the surface of an adiabatic half-space is surrounded by circular ring source images which are to be chosen such that

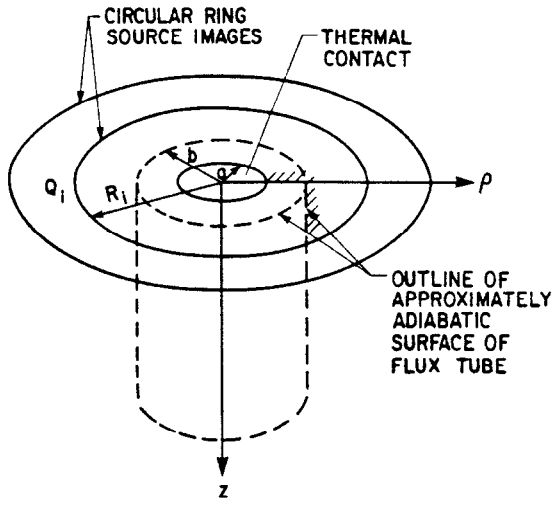

Fig. 2 Arrangement of ring source images around a circular contact to simulate a circular flux tube

an approximately adiabatic surface at $\rho=b$ will result. Although the thermal constriction resistance parameter, ψ, is based on a flux tube of semi-infinite length, it will be seen that only a "small" finite length of the approximately adiabatic flux tube need be considered to give accurate results. By using this approach the adiabatic boundary condition at $\rho=b$ of an approximate flux tube can be formulated such that a finite number of optimised circular ring source images can be chosen by non-linear optimisation.

For the true semi-infinite circular flux tube [5], the governing differential equation and boundary conditions are

$$\nabla^2 T = 0 \tag{1}$$

$$\text{where } \nabla^2 \equiv \frac{1}{\rho}\frac{\partial}{\partial \rho}\left(\rho\frac{\partial}{\partial \rho}\right) + \frac{\partial^2}{\partial z^2} \tag{2}$$

Also,

$$\frac{\partial T}{\partial \rho}(0,z) = 0 \quad , \quad 0 \leq z < \infty \tag{3}$$

$$\frac{\partial T}{\partial \rho}(b,z) = 0 \quad , \quad 0 \leq z < \infty \tag{4}$$

$$T \to 0 \quad \text{as} \quad (\rho^2+z^2)^{1/2} \to \infty \tag{5}$$

$$\frac{\partial T}{\partial z}(\rho,0) = 0 \quad \text{outside contact area} \tag{6}$$

where b is the radius of the flux tube.

Note that both the circular contact on a half-space and the circular ring sources on a half-space have temperature fields which satisfy all of the above except Eq. (4). In addition for the circular contact we have the last necessary condition for the flux tube that

$$-k\frac{\partial T}{\partial z}(\rho,0) = q_o \quad , \quad 0 \leq \rho \leq a \tag{7}$$

where q_o is some specified uniform flux over the contact area and a is the radius of the circular contact.

Thus by superposing solutions the temperature rise at any point in the half-space is

$$T(\rho,z) = T^c(\rho,z) + \sum_{i=1}^{M} T_i^r(\rho,z) \tag{8}$$

where $T^c(\rho,z)$ is the temperature field due to a circular contact on a half-space, $T_i^r(\rho,z)$ is the temperature field due to the i^{th} circular ring image and M is the number of ring images.

The radial flux at $\rho=b$ can be written as

$$-k\frac{\partial T}{\partial \rho}(b,z) = \left[-k\frac{\partial T^c}{\partial \rho}(b,z)\right] + \sum_{i=1}^{M}\left[-k\frac{\partial T_i^r}{\partial \rho}(b,z)\right] \tag{9}$$

The first term on the right-hand side of Eq. (9) is a function of a,b,z and q_o and can be treated as a "known" quantity given by Eq. (A-9) at $\rho=b$. This term is written as

$$q^c = -k\frac{\partial T^c}{\partial \rho}(b,z) \tag{10}$$

The second term on the right-hand side of Eq. (9) is a function of b,z and the "unknown" quantities Q_i and R_i. Thus Eq. (9) is written as

$$-k\frac{\partial T}{\partial \rho}(b,z) = q^c + \sum_{i=1}^{M} Q_i\, g(R_i) \tag{11}$$

where $g(R_i)$ is a non-linear relationship connecting R_i to the radial flux at some point P(b,z).

The exact boundary condition that Eq. (11) should mimic is Eq. (4). However if some residual boundary-flux e_j is accepted at a "test-point" z_j then the approximate boundary condition is

$$e_j = q_j^c + \sum_{i=1}^{M} Q_i\, g_j(R_i) \tag{12}$$

where it is assumed that e_j will be made "small" in some sense.

The important remaining point is the required length of the flux tube which must be set approximately adiabatic. Some insight to this length can be made by comparing the works of [16] and [5]. From this a finite flux tube behaves like a semi-infinite flux tube in terms of its constriction parameter ψ when $\tanh(\delta_1\alpha)=1$, where δ_1, is the first root of $J_1(\delta_n) = 0$ ($\delta_1 \approx 3.83$) and α is the ratio of the length of the finite flux tube to its flux tube radius b. For example if $\alpha=1$, then $\tanh(\delta_1\alpha) \approx .9991$, $\alpha = 1.5$, $\tanh(\delta_1\alpha) \approx .99998$, and $\alpha = 2$, $\tanh(\delta_1\alpha) \approx .9999996$. Thus fitting a perfectly adiabatic boundary to a length of b should result in a maximum error of less than .1% in the constriction parameter. In every case for the results that follow a length of b was used with great success. Lengths of 1.5b and 2b were also tried for cases where some error in ψ was present but no improvement was ever seen for a given number of annular ring images.

Thus if N test-points are considered over the finite domain $0 \le z \le b$, then the sum of residual boundary-fluxes squared is

$$E_t = \sum_{j=1}^{N}\left\{q_j^c + \sum_{i=1}^{M} Q_i\, g_j(R_i)\right\}^2 \tag{13}$$

For a uniform flux over the circular contact area q_j^c is given by Eq. (A-11) at $\rho=b$ or

$$q_j^c = q_o\frac{b}{a}\sum_{i=1}^{\infty} A_{2n}\left(\frac{a}{[b^2+z_j^2]^{1/2}}\right)^{2n+1}$$
$$\left\{(2n-1)P_{2n-2}(\tau_j) + \tau_j C_{2n-3}^{3/2}(\tau_j)\right\} \tag{14}$$

where $\tau_j \equiv z_j/(b^2+z_j^2)^{1/2}$ (15)

and A_{2n} is given by Eq. (A-8) and $P_{2n-2}(\cdot)$ and $C_{2n-3}^{3/2}(\cdot)$ are Legendre and Gegenbauer polynomials [14].

In addition from Eq. (A-26)

$$g_j(R_i) = \frac{2R_i}{\pi}\left\{\frac{b+R_i}{\sigma_{ij}^{3/2}}K(\lambda_{ij}) + \frac{\sigma_{ij}-b(2b+2R_i)}{2b\sigma_{ij}^{3/2}}\right.$$
$$\left.[E(\lambda_{ij})/(1-\lambda_{ij}^2)-K(\lambda_{ij})]\right\} \tag{16}$$

where $\sigma_{ij} \equiv z_j^2 + (b+R_i)^2$ (17)

$$\lambda_{ij} \equiv 2(bR_i/\sigma_{ij})^{1/2} \tag{18}$$

and $K(\cdot)$ and $E(\cdot)$ are complete elliptic integrals of the first and second kinds.

Finally, the z_j are chosen by 11 equally spaced test-points between $z_o=0$ and $z_{11}=b$. Other numbers of test-points such as 16 and 21 for the test domain $0 \le z_j \le b$ were also tried but no noticeable change in ψ was observed.

Thus the proper selection of Q_i and R_i and ultimately the solution of the problem is found by minimizing E_t. For the results contained in this report, the non-linear FORTRAN-60 routine GAUSHAUS [15] was used.

Presentation and Discussion of Results

The solution to the optimization problem posed by minimizing E_t in Eq. (13) is a "best" selection of sizes and source strengths of circular ring images. After determining these sizes and strengths, the quantity of interest is the dimensionless thermal constriction resistance parameter defined as

$$\psi \equiv 4ka\, R_c \tag{19}$$

where R_c is the thermal constriction resistance given by

$$R_c = \frac{\bar{T}_c - \bar{T}(z=L)}{Q^c} - R_m \tag{20}$$

where $\bar{T}_c$ is the average temperature rise on the contact, $\bar{T}(z=L)$ is the average temperature rise at any depth L, Q^c is the total heat flux on the contact, and R_m is the "material" resistance from z=0 to z=L given by

$$R_m = L/kA_t \tag{21}$$

where A_t is the total cross-sectional area of the flux tube, πb^2. Thus

$$\psi = \frac{4ka}{Q^c}(\bar{T}_c - \bar{T}(z=L)) - \frac{4aL}{\pi b^2} \qquad (22)$$

where $$Q^c = \pi a^2 q_o \qquad (23)$$

The average contact temperature can be calculated easily using a Gaussian quadrature scheme to integrate numerically the temperature rise due to the circular ring images. The contribution to $\bar{T}_c$ from the circular contact is $(8/3\pi)(q_o a/k)$ for the uniform flux.

The average temperature rise at some flux tube plane z=L can also be calculated easily using a Gaussian quadrature scheme to integrate numerically the temperature rises due to both the circular contact and the circular ring images. Although any value of $L \leq b$ can be used, a value of .8b was used in the results that follow because the nearly uniform temperature at this flux tube plane allows easy integration by Gauss quadrature.

The results for the constriction parameter over the range $.01 < \varepsilon < 9$, where ε is the dimensionless contact size, $\varepsilon \equiv a/b$, are contained in Table 1 for one, two or three optimised circular ring images. The analytical solution reported in Table 1 comes from [5].

The procedure to obtain a given ψ in Table 1 consisted first of running the non-linear optimisation routine GAUSHAUS [15] on the University of Waterloo IBM 4341 mainframe system in compiled FORTRAN-66 to minimize the sum of boundary-flux residuals, E_t. From this program the corresponding circular ring image source strengths and radii were then recorded and inputted to a compiled Microsoft BASIC routine on an IBM-PC. This program calculates the constriction parameter ψ, the residual boundary-fluxes, and summarizes each run.

Overall the method of optimised images worked very well for this problem. With only one circular ring image, an engineering accuracy of 1% or less was obtained up to $\varepsilon = .6$. Even at a large contact size of $\varepsilon = .8$ the error in ψ was only 7%. When a second optimised image is added even better accuracy in ψ for large ε can be obtained. And when a third optimised image is included, complete four decimal place agreement in ψ is seen for all $\varepsilon \leq .9$.

The mainframe execution time for one optimised circular ring was typically .3 - .5 seconds. With two images the typical time was 1.2 - 1.8 seconds and with three images 5 - 7 seconds. Obviously since only one image was needed for small relative contact sizes ($\varepsilon<.5$), the method of optimised images is most economical in this range. This makes sense because the field for a small contact in a flux tube is essentially a minor perturbation of the half-space solution. At large relative contact sizes the temperature field is substantially different from that of a contact on a half-space and consequently more optimised images are needed.

In order to compare the accuracy of the results of the circular contact on a circular flux tube to other flux tube problems where analytical solutions are impractical or unavailable, an attempt will be made to relate accuracy in ψ to the residual boundary-flux, e_j. From Eq. (12) the residual boundary-fluxes e_j can be calculated after the optimisation process is completed. However e_j is dimensional and has a decreasing effect on ψ at increasing depths. Thus a relative residual boundary-flux, ϕ_j is defined as the ratio of residual boundary-flux to the flux which would be present from a contact on a half space alone, or

$$\phi_j \equiv (e_j/q_j^c) \times 100\%$$

For a dimensionless contact size, $\varepsilon \equiv a/b$, of .2, .5 and .8, the relative residual boundary-fluxes have been tabulated in Table 2 for the case of one and two optimised circular ring images.

z_j	ε =.2		ε =.5		ε =.8	
	NR=1	NR=2	NR=1	NR=2	NR=1	NR=2
0.0	2.50	.001	4.21	.102	11.14	0.33
.1	2.08	.000	3.32	.032	6.85	-0.17
.2	0.90	-.001	0.96	-.115	-2.50	-0.43
.3	-0.77	.000	-2.17	-.224	-11.56	-0.38
.4	-2.55	.002	-5.16	-.246	-17.22	-0.94
.5	-3.83	.027	-5.94	.849	-8.11	6.47
.6	-4.44	-.002	-7.13	-.195	-13.55	-3.35
.7	-3.49	-.013	-4.72	-.212	-3.87	-3.86
.8	-0.61	-.023	0.62	-.224	10.57	-2.96
.9	4.62	-.016	9.13	-.119	29.22	-0.06
1.0	12.53	.042	20.95	.279	51.48	5.31

Table 2. Relative residual boundary-fluxes ϕ_j in % for a concentric circular flux tube with uniform flux

At a small contact size such as ε=.2, relative residual boundary-fluxes have very little effect on the accuracy of ψ. For example, adding a second optimised circular ring image dropped the relative residual boundary-fluxes at least 2 orders of magnitude but ψ only changed from .8011 to .8009.

At an intermediate contact size such as ε=.5 the relative residual boundary-fluxes begin to have

Number of Optimised Ring Images	Constriction Parameter, $\psi \equiv 4kaR_c$ ($\varepsilon \equiv a/b$)										
	ε =.01	ε =.05	ε =.1	ε =.2	ε =.3	ε =.4	ε =.5	ε =.6	ε =.7	ε =.8	ε =.9
1	1.0667	1.0104	.9402	.8011	.6652	.5342	.4101	.2952	.1928	.1074	.0526
2	-	-	.9401	.8009	.6649	.5338	.4094	.2940	.1904	.1025	.0379
3	-	-	-	-	-	.5337	.4092	.2936	.1895	.1008	.0331
Analytical Solution	1.0667	1.0104	.9401	.8009	.6649	.5337	.4092	.2936	.1895	.1008	.0331

Table 1. Constriction parameter ψ of a concentric circular flux tube with uniform flux

an effect. However even though the average relative residual boundary flux is about 6% with one image, the error in ψ is about .2%. Adding the second optimised annular ring image brings the relative residual boundary-fluxes down to less than .3% and virtually eliminates all error in ψ.

When the contact size becomes quite large, such as ε=.8, the constriction parameter ψ becomes very sensitive to the relative residual boundary-fluxes. For example at ε=.8 with a uniform contact flux an average relative residual boundary-flux of 14% for one image gave 7% error in ψ and 2.2% for two images gave 1.7% error in ψ. When a third optimised image was included, the average residual boundary-flux was about .08% and all error in ψ was eliminated. Thus at large contact sizes not only are more optimised images required to produce a certain level of relative residual boundary-flux, but in addition a given level of relative residual boundary-flux causes greatest error in ψ at these large contact sizes. However even for such large contact sizes, good engineering accuracy of 2% error or less in ψ should be obtained by using enough optimised images to reduce the average residual boundary-flux to 2-4% or less.

In general for small and intermediate contact sizes ($\varepsilon \leq .6$), accurate results for the constriction parameter ψ can be obtained even with typical relative residual boundary-fluxes of 5-10%. This fact is important to ensure reliable results when solving problems where it is impractical or impossible to continue adding optimised images until a "convergence" in ψ is reached.

In Table 3 the actual optimised circular ring source images are tabulated for several optimisation cases. Note that the dimensional results for Q_i and R_i in Table 3 are based on a uniform contact flux of $q_o = 1$, a thermal conductivity k=1 and a flux tube radius b=1.

Optimisation Case	Ring Image No. i	Source Strength Q_i	Ring Radius R_i
ε =.2, 1 image	1	.1826	2.3915
ε =.5, 1 image	1	1.0540	2.2505
ε =.8, 1 image	1	2.3148	1.9864
ε =.2, 2 images	1 2	.3676 .0629	5.0408 1.8886
ε =.5, 2 images	1 2	1.7341 .2682	3.8906 1.6829
ε =.8, 2 images	1 2	3.1615 .2933	2.7476 1.3271
ε =.5, 3 images	1 2 3	2.2594 .2812 .0857	4.8835 1.8875 1.5531
ε =.8, 3 images	1 2 3	4.7034 .5384 .1425	3.9975 1.6408 1.2646

Table 3. Optimised circular ring source images for a concentric circular flux tube with uniform flux

CONSTRICTION RESISTANCE OF CIRCULAR CONTACTS ON SQUARE FLUX TUBES BY OPTIMISED IMAGES

Formulation of Boundary Condition for Approximate Flux Tube

For the semi-infinite flux tube of square cross-section with a concentric circular contact, the governing differential equation and boundary conditions are

$$\nabla^2 T = 0 \tag{24}$$

where $$\nabla^2 \equiv \frac{\partial^2}{\partial x^2} + \frac{\partial^2}{\partial y^2} + \frac{\partial^2}{\partial z^2} \tag{25}$$

$$\left.\begin{aligned} &\frac{\partial T}{\partial x}(0,y,z) = 0 \quad \text{for} \quad -\infty < y < \infty \\ &\frac{\partial T}{\partial y}(x,0,z) = 0 \quad \text{for} \quad -\infty < x < \infty \end{aligned}\right\} \; 0 \leq z < \infty \tag{26}$$

$$\left.\begin{aligned} &\frac{\partial T}{\partial x}(\pm b,y,z) = 0 \quad \text{for} \quad -b \leq y \leq b \\ &\frac{\partial T}{\partial y}(x,\pm b,z) = 0 \quad \text{for} \quad -b \leq x \leq b \end{aligned}\right\} \; 0 \leq z < \infty \tag{27}$$

$$T(x,y,z) \to 0 \quad \text{as} \quad (x^2+y^2+z^2)^{1/2} \to \infty \tag{28}$$

$$\frac{\partial T}{\partial z}(x,y,0) = 0 \quad \text{outside contact area} \tag{29}$$

Note that the circular contact on a half-space and collection of four finite-lines as shown in Fig. 3 each satisfy all these conditions except Eq. (27). In addition for the circular contact on a half-space we have the last necessary condition for the flux tube that

$$-k \frac{\partial T}{\partial z}(x,y,0) = f(\rho) \quad \text{for} \quad 0 \leq \rho \leq a \tag{30}$$

where $\rho = (x^2+y^2)^{1/2}$ and $f(\rho)$ is some specified flux distribution on the contact such as uniform or equivalent isothermal.

Because of the symmetry of the problem only one finite-line source per flux tube side need be considered. In addition test-points for the symmetric boundary conditions given by Eq. (27) can be chosen from only one half of one side of the flux tube. As shown in Fig. 4 the domain $0 \leq x \leq b$, y=b has been chosen and the ideal boundary condition to be satisfied is

$$-k \frac{\partial T}{\partial y}(x,b,z) = 0 \quad 0 \leq x \leq b, \quad 0 \leq z < \infty \tag{31}$$

By using the methods of the previous section, this exact boundary condition can be rewritten in terms of an approximate one for which a residual boundary-flux at the j_{th} test-point is

$$e_j = q_j^c + \sum_{i=1}^{M} Q_i \, g_j(y_{oi}, \ell_i) \tag{32}$$

where q_j^c is the flux normal to y=b at the test-point $P(x_j,b,z_j)$ due to the circular contact and is given by Eqs. (A-4) or (A-11) depending on the flux case, M is the number of optimised finite-line images on one side of the flux tube, or alternatively, the number of sets of four symmetric

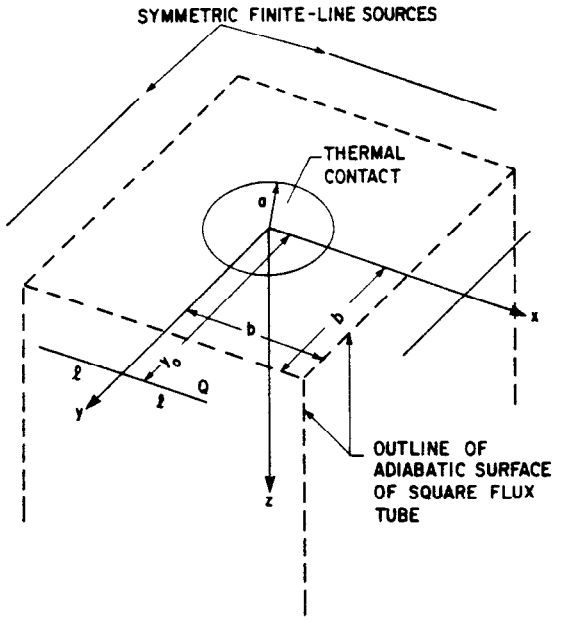

Fig. 3 Arrangement of finite-line source images around a circular contact to simulate a square flux tube

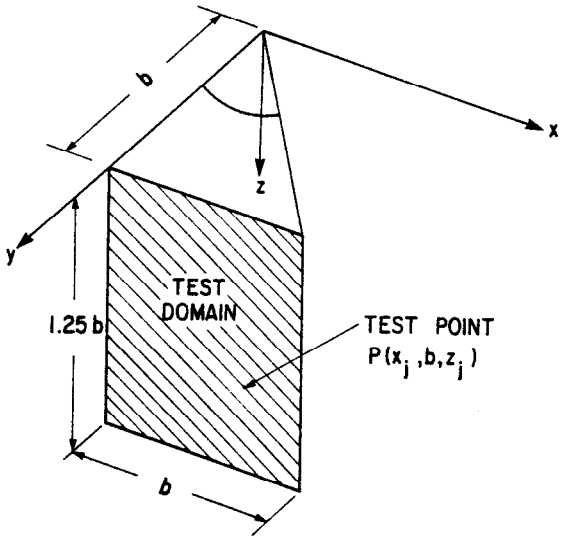

Fig. 4 Required test domain for a square flux tube

finite-line images, Q_i is the line strength of the i^{th} optimised finite-line image, and $g_j(y_{oi},\ell_i)$ is a nonlinear relationship formed from Eqs. (A-17) and (A-22) to describe the flux at the test-point $P(x_j,b,z_j)$ from a finite-line set with a half-length of ℓ_i and a distance of y_{oi} from the origin. As discussed in the previous section, the flux tube length need not extend to infinity to give accurate results in terms of the thermal constriction resistance. After some experimentation it was found that no improvements in the accuracy of the constriction resistance occurred by considering approximate flux tube lengths greater than 1.25b. This length was used for all square flux tube results which follow. Note that for a square flux tube of half-width b, a circular flux tube of equal cross-sectional area would have a radius of 1.13b. Since in the previous section a flux tube length of b was considered for a circular flux tube of radius b, a flux tube length of 1.25b in this case also seems reasonable based on the previous experience.

As in the concentric circular flux tube problem, the correct images are determined by minimizing the total sum of residual boundary-fluxes squared given by

$$E_t = \sum_{j=1}^{N} \{q_j^c + \sum_{i=1}^{M} Q_i\, g_j(y_{oi},\ell_i)\}^2 \qquad (33)$$

Again the non-linear FORTRAN-60 routine GAUSHAUS [15] will be used to minimize E_t. Note that each set of four symmetric optimised finite-line images has 3 unknown parameters as opposed to only 2 unknown parameters for each optimised circular ring image of the previous problem.

Within the test domain of Fig. 4 the test-points are chosen by 5 equally spaced points between $0 \le x_j \le b$ and 6 equally spaced points between $0 \le z_j \le 1.25b$. Thus 30 test-points are used to cover the test-domain shown in Fig. 4. Other larger numbers of test-points were tried, especially for the dimensionless contact size $\varepsilon \equiv a/b = .5$, but no noticeable change in the constriction parameter ψ was observed.

Presentation of Results

As in the previous problem the integrated parameter of interest after minimizing E_t is the dimensionless thermal constriction resistance parameter. Again this is defined as

$$\psi \equiv 4kaR_c \qquad (34)$$

or after defining R_c as in Eq. (19) and noting that the cross-sectional area of the square flux tube is $4b^2$ then

$$\psi \equiv \frac{4ka}{Q^c}(\bar{T}_c - \bar{T}(z=L)) - \frac{aL}{b^2} \qquad (35)$$

where $\bar{T}_c$ is the average contact temperature rise, $\bar{T}(z=L)$ is the average temperature rise in some flux tube cross-sectional plane $z=L$, Q^c is the total flux over the contact area ($Q^c = 4kT_o a$ for the equivalent isothermal flux or $Q^c = \pi a^2 q_o$ for the uniform flux), and L for the results which follow has been set at L=b.

The quantities $\bar{T}_c$ and $\bar{T}(z=L)$ are again calculated by Gaussian quadrature using the temperature rises expressions for circular contacts and finite-line sources on a half-space, as given in the Appendix.

The computation procedure for both the equivalent isothermal and uniform flux cases on the circular contact on a square flux tube is identical to the previous concentric circular flux tube procedure.

For the equivalent isothermal flux case, q_j^c of Eq. (33) is given by

$$q_j^c = \frac{4kT_o a}{\pi}\left(\frac{b}{\rho}\right)\left\{\frac{\rho-a}{\sigma_1} + \frac{\rho+a}{\sigma_2}\right\}$$

$$\left\{(\sigma_1+\sigma_2)[(\sigma_1+\sigma_2)^2 - 4a^2]^{1/2}\right\}^{-1} \qquad (36)$$

where $\rho \equiv (x_j^2 + b^2)^{1/2}$ (37)

$$\sigma_1 \equiv [(\rho-a)^2 + z_j^2]^{1/2} \quad (38)$$

$$\sigma_2 \equiv [(\rho+a)^2 + z_j^2]^{1/2} \quad (39)$$

In Table 4 the resultant values of ψ for the equivalent isothermal flux case are tabulated for one, two or three sets of four symmetric finite-line images over the range of the dimensionless contact size $\varepsilon \equiv a/b$, $.01 \leq \varepsilon \leq .9$. Note that no analytical solution is presently available for the constriction resistance of a circular contact on a square flux tube with an equivalent isothermal flux distribution. However all the results in Table 4 do seem to be converging to the accuracy shown.

For the uniform flux case, q_j^c of Eq. (33) is given by

$$q_j^c = \frac{q_o b}{a} \sum_{n=1}^{\infty} A_{2n} \left(\frac{a}{[\rho^2+z_j^2]^{1/2}}\right)^{2n+1} \{(2n-1)\, P_{2n-2}(\tau_j) + \tau_j C_{2n-3}^{3/2}(\tau_j)\} \quad (40)$$

where $\tau_j \equiv z_j/(\rho^2+z_j^2)^{1/2}$ (41)

$$\rho \equiv [b^2+z_j^2]^{1/2} \quad (42)$$

with A_{2n} as in Eq. (A-8) and $P_{2n-2}(\cdot)$ and $C_{2n-3}^{3/2}(\cdot)$ are Legendre and Gegenbauer polynomials [14].

The results for the constriction parameter ψ for the uniform flux case are contained in Table 5 for one, two or three sets of four symmetric finite-line images. The reference answer reported in Table 5 is the "corrected Beck expression" [17,18]

$$\psi = 1.0808 - 1.2415\varepsilon + .1797\varepsilon^3 \quad (43)$$

where ε is the dimensionless contact size, $\varepsilon \equiv a/b$. Because Eq. (43) is not valid to the accuracy reported in Table 5 for $\varepsilon \geq .5$, the reference answer numbers in brackets are only estimates. Again excellent convergence in ψ for the accuracy shown is observed.

Discussion and Correlation of Results

Once again the method of optimised images has worked well overall. Good convergence of the results for the accuracy shown was observed using up to three optimised sets of four symmetric finite-line images.

As anticipated, accurate results were most easily obtained for small contact sizes. In fact using only one set of optimised images on the uniform flux case, .1% error in ψ was observed at ε=.2, .8% error at ε=.5 and 6.8% error at ε=.8.

When a second set of four symmetric finite-line images was added, all error in ψ was eliminated for the accuracy shown in the range $.01 \leq \varepsilon \leq .9$. The addition of a third set of finite-lines merely confirmed that converged results had been obtained.

An examination of the relative residual boundary-fluxes for each ψ in Tables 4 and 5 showed similar trends in accuracy of ψ relative to boundary residuals as seen for the circular flux tubes.

The results of this work for the constriction

Number of Optimised Finite-Line Images[a]	Constriction Parameter, $\psi \equiv 4kaR_c$ ($\varepsilon \equiv a/b$)										
	ε =.01	ε =.05	ε =.1	ε =.2	ε =.3	ε =.4	ε =.5	ε =.6	ε =.7	ε =.8	ε =.9
1	.988	.938	.876	.755	.636	.521	.412	.311	.221	.148	.106
2	-	-	.876	.754	.633	.517	.407	.303	.210	.129	.067
3	-	-	-	-	-	-	-	.303	.210	.129	.065

Table 4. Constriction parameter ψ for a circular contact with equivalent isothermal flux on a square flux tube

Note (a): Refers to the number of sets of four symmetric finite-line source images as shown in Fig. 2.

Number of Optimised Finite-Line Images[a]	Constriction Parameter, $\psi \equiv 4kaR_c$ ($\varepsilon \equiv a/b$)										
	ε =.01	ε =.05	ε =.1	ε =.2	ε =.3	ε =.4	ε =.5	ε =.6	ε =.7	ε =.8	ε =.9
1	1.068	1.019	.957	.835	.715	.599	.488	.383	.288	.205	.144
2	-	-	.957	.834	.713	.596	.484	.377	.279	.192	.120
3	-	-	-	-	-	-	-	.377	.279	.192	.120
Reference Answer	1.068	1.019	.957	.834	.713	.596	(.484)	(.377)	(.28)	(.19)	(.1)

Table 5. Constriction parameter ψ for a circular contact with uniform flux on a square flux tube

Note (a): Refers to the number of sets of four symmetric finite-line source images as shown in Fig. 2.

parameter also represent useful data for research in contact resistance. Thus for convenient engineering purposes, a correlation of the results for both contact conditions on the square flux tube and those for uniform flux on a concentric circular flux tube will be made. A correlation of the results from the equivalent isothermal flux case on the circular flux tube is unnecessary because the true isothermal constriction parameter was correlated in [4]. The form of the correlation in [4] will be used again to give ψ as a function of ε. This correlation is

$$\psi = \psi_\infty + C_1\varepsilon + C_3\varepsilon^3 + C_5\varepsilon^5 + C_7\varepsilon^7 \qquad (44)$$

where $\varepsilon \equiv a/b$, a is the contact radius, b is the flux tube radius for the concentric circular flux tube or the half-width of the square flux tube, and ψ_∞ is the constriction parameter for a circular contact on a half-space ($\varepsilon=0$).

The coefficients of Eq. (44) are given in Table 6. The resultant correlations all have no error with respect to their input data when rounded-off appropriately.

CONCLUSIONS

For most practical flux tube problems in contact resistance where both the contact and flux tube cross-section are modelled as circular, square, elliptical, rectangular, etc., the method of optimised images can be used to determine the constriction resistance parameter accurately with a relatively small computational effort.

Since resistance is defined by average temperatures and total heat flux, that is, integrated quantities, then the effect of deviations from the exact adiabatic boundary condition at the flux tube sides tends to cancel out in terms of the integrated results. Thus the thermal constriction resistance parameter approaches its exact value while the imposed adiabatic boundary condition is still only approximately satisfied. Furthermore the temperatures calculated from the optimised images are most accurate near the contact where thermal gradients are highest and the temperature field is most complex. Such high gradient accuracy is important both for component design where thermal stresses are of major concern and for analogous electrical problems where high voltage gradients can cause degradation of material properties.

Even though the constriction resistance parameter used for contact resistance is based on a flux tube of semi-infinite length, for calculation purposes using the method of optimised images, only a relatively small finite length flux tube need be considered for accurate results. From the experience gained in producing the numerical results which appear in this work, a finite length approximately equal to the largest "radius" in the flux tube cross-section seems to suffice.

Finally two flux tube problems in contact resistance which may now be solved by the optimised images technique are the elliptical contact on a rectangular flux tube and the elliptical contact on an elliptical flux tube. Solution should be possible for both by superposing an isothermal elliptical contact and several finite-line source images on a half-space according to an optimised images criterion.

ACKNOWLEDGEMENTS

The authors thank Mr. J. DeVaal of the Dept. of Mechanical Engineering and Prof. Y.L. Chow of the Dept. of Electrical Engineering at the University of Waterloo for their comments and suggestions. The authors also acknowledge the financial support of the National Science and Engineering Reseach Council of Canada under operating grant A-7455 for Dr. Yovanovich.

REFERENCES

[1] Cooper, M., Mikic, B.B., and Yovanovich, M.M., "Thermal Contact Conductance", International Journal of Heat and Mass Transfer, Vol. 12, Jan. 1969, pp. 279-300.

[2] McGee, G., "An Analytical and Experimental Study of the Heat Transfer Characteristics of Cylinders - Flat Contacts", M.A.Sc. Thesis, University of Waterloo, 1982.

[3] DeVaal, J., Ph.D. Thesis in progress, University of Waterloo, 1984.

[4] Negus, K.J., and Yovanovich, M.M., "Constriction Resistance of Circular Flux Tubes with Mixed Boundary Conditions by Linear Superposition of Neumann Solutions", 22nd ASME Heat Transfer Conference, Niagara Falls, N.Y., Aug. 6-8, 1984.

[5] Yovanovich, M.M., "General Expressions for Circular Constriction Resistances for Arbitrary Flux Distributions", AIAA 13th Aerospace Sciences Meeting, Pasadena, California, Jan. 20-22, 1975.

[6] Smythe, W.R., Static and Dynamic Electricity, McGraw-Hill, New York, 1950.

[7] Panofsky, W.K.H., and Phillips, M., Classical Electricity and Magnetism, Addison-Wesley, New York, 1956.

Flux Tube Geometry and Contact Boundary Condition	ψ_∞	C_1	C_3	C_5	C_7
Circle/Circle Uniform Flux	1.08076	-1.41042	.26604	-.00016	.058266
Circle/Circle[(a)] True Isothermal	1.00000	-1.40978	.34406	.04305	.02271
Circle/Square Uniform Flux	1.08076	-1.24110	.18210	.00825	.038916
Circle/Square Equiv. Isothermal Flux	1.00000	-1.24142	.20988	.02715	.02768

Table 6. Coefficients for correlations of the constriction parameter ψ
Note(a): This correlation is given in [4].

[8] Kellogg, O.D., Foundations of Potential Theory, Dover, New York, 1953.
[9] Chow, Y.L., and Charalambous, C., "Static-Field Computations by the Method of Optimised Simulated Images", Proc. IEEE, Vol. 126, No. 1, Jan. 1979, pp. 123-125.
[10] Fletcher, R., "A New Approach to Variable Metric Algorithms", Computing Journal, Vol. 13, 1970, pp. 317-322.
[11] Chow, Y.L., Lan, Y.F., and Fang, D.G., "Capacitance and its Upper and Lower Bounds by the Method of Optimised Simulated Images", J. Applied Physics, Vol. 53, No. 11, November, 1982, pp. 7144-7148.
[12] Carslaw, H.S., and Jaeger, J.C., Conduction of Heat in Solids, Oxford, London, 1959.
[13] Yovanovich, M.M., and Martin, K.A., "Some Basic Three-Dimensional Influence Coefficients for the Surface Element Method", AIAA 15th Thermophysics Conference, Snowmass, Colorado, July 14-16, 1980.
[14] Abramowitz, M., and Stegun, I.A., Handbook of Mathematical Functions, Dover, New York, 1972.
[15] Wolfe, P.J. and Meeter, D.A., "Non-Linear Least Squares (GAUSHAUS)", University of Wisconsin Computing Center, December, 1965.
[16] Yovanovich, M.M., Tien, C.H , and Schneider, G.E., "General Solution of Constriction Resistance within a Compound Disk", AIAA 17th Aerospace Sciences Meeting, New Orleans, Louisiana, Jan. 15-17, 1979.
[17] Beck, J.V., "Effects of Multiple Sources in the Contact Conductance Theory", ASME Journal of Heat Transfer, Vol. 101, pp. 132-136, Feb. 1979.
[18] Negus, K.J., and Yovanovich, M.M., Personal letters to J.V. Beck, Dec. 1983.

APPENDIX - TEMPERATURE RISE AND FLUX OF CONTACTS AND IMAGES ON AN ADIABATIC HALF-SPACE

Circular Contact-Equivalent Isothermal Flux

For the circular contact area on an adiabatic half-space as shown in Fig. 5, the expressions for temperature rise and flux at some point $P(\rho,z)$ are functions solely of the contact boundary conditions. In this case the contact condition is set isothermal which creates a mixed boundary value problem in the polar cylindrical coordinate system of Fig. 5. However, the problem is one-dimensional in an oblate spheroidal coordinate system and the solution is given simply by [6,12] as

$$T(\rho,z) = \frac{2T_o}{\pi} \sin^{-1}(\beta) \qquad (A\text{-}1)$$

where $$\beta = \frac{2a}{[(\rho-a)^2+z^2]^{1/2}+[(\rho+a)^2+z^2]^{1/2}} \qquad (A\text{-}2)$$

and as shown in Fig. 5, T_o is the specified isothermal contact temperature and a the radius of the circular contact.

From Eq. (A-1) the equivalent isothermal flux can be easily found by differentiation with respect to z along z=0, $0 \le \rho \le a$ and is

$$q = 2kaT_o(1-(\rho/a)^2)^{-1/2} \qquad (A\text{-}3)$$

where k is the homogeneous thermal conductivity of the semi-infinite solid of Fig. 5.

For work in "creating" flux tubes by optimised images, the radial flux of this temperature field is required for any location. This flux can be found

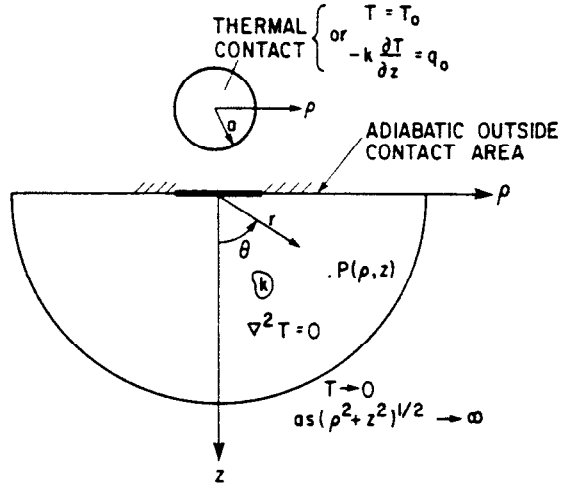

Fig. 5 Circular contact on an adiabatic half-space

by simple differentiation of Eq. (A-1) with respect to ρ and is given by

$$-k\frac{\partial T}{\partial \rho}(\rho,z) = \frac{4kT_o a}{\pi}\left\{\frac{\rho-a}{\sigma_1}+\frac{\rho+a}{\sigma_2}\right\}$$
$$\{(\sigma_1+\sigma_2)[(\sigma_1+\sigma_2)^2-4a^2]^{1/2}\}^{-1} \qquad (A\text{-}4)$$

where $$\sigma_1 \equiv [(\rho-a)^2+z^2]^{1/2} \qquad (A\text{-}5)$$

$$\sigma_2 \equiv [(\rho+a)^2+z^2]^{1/2} \qquad (A\text{-}6)$$

Circular Contact-Uniform Flux

If the circular contact of Fig. 5 is subjected to a uniform prescribed flux, q_o, then the temperature rise in an r-θ spherical coordinate system is [13] for $r \ge a$

$$T(r,\theta) = \frac{q_o a}{k}\sum_{n=1}^{\infty} A_{2n}\left(\frac{a}{r}\right)^{2n-1} P_{2n-2}(\cos\theta) \qquad (A\text{-}7)$$

where $P_{2n-2}(\cdot)$ is a Legendre polynomial of order 2n-2 and A_{2n} is given by

$$A_{2n} = (-1)^{n+1}\frac{1\cdot3\cdot5\cdot\ \ldots\ldots\ldots\ldots(2n-3)}{2\cdot4\cdot6\cdot\ \ldots\ldots\ldots\ldots\ (2n)} \qquad (A\text{-}8)$$

But in the polar cylindrical coordinate system of Fig. 5,

$$r = [\rho^2+z^2]^{1/2}, \qquad \cos\theta = z/[\rho^2+z^2]^{1/2}$$

And thus the temperature rise for a circular contact on an adiabatic half-space subjected to uniform flux is for $r \ge a$

$$T(\rho,z) = \frac{q_o a}{k}\sum_{n=1}^{\infty} A_{2n}\left[\frac{a}{(\rho^2+z^2)^{1/2}}\right]^{2n-1} P_{2n-2}(\tau) \qquad (A\text{-}9)$$

where $$\tau \equiv z/(\rho^2+z^2)^{1/2} \qquad (A\text{-}10)$$

Again the radial flux for this field can be determined by differentiation with respect to ρ to give

$$-k\frac{\partial T}{\partial \rho}(\rho,z) = q_o \left(\frac{\rho}{a}\right) \sum_{n=1}^{\infty} A_{2n} \left[\frac{a}{(\rho^2+z^2)^{1/2}}\right]^{2n+1}$$

$$\{(2n-1)\, P_{2n-2}(\tau) + \tau\, C_{2n-3}^{3/2}(\tau)\} \qquad \text{(A-11)}$$

where $C_{2n-3}^{3/2}(\cdot)$ is a Gegenbauer or Ultraspherical polynomial as described in [14].

Note that when n=1,

$$P_o(x) = 1, \text{ or } \frac{dP_o}{dx}(x) = 0$$

and thus for our purposes $C_{-1}^{3/2}(x)$ $\left(= \frac{dP_o(x)}{dx}\right)$ will be set to zero.

If r < a then from [13]

$$T(\rho,z) = \frac{q_o a}{k}\left\{1 - \frac{z}{a} + \sum_{n=1}^{\infty} A_{2n} \left(\frac{r}{a}\right)^{2n} P_{2n}(\tau)\right\} \qquad \text{(A-12)}$$

However this expression was not needed in this work.

Finite-Line Image Source

For a finite-line image source of line strength Q and half-length ℓ which is aligned parallel to the x-axis, bisected by the y-axis and located on the surface of an adiabatic half-space shown in Fig. 6, the temperature rise can be easily shown to be [8]

$$T(x,y,z) = \frac{Q}{2\pi k} \ell n\left\{\frac{\sigma_{x1} + x + \ell}{\sigma_{x2} + x - \ell}\right\} \qquad \text{(A-13)}$$

where $\sigma_{x1} = [(x+\ell)^2 + (y-y_o)^2 + z^2]^{1/2}$ (A-14)

$$\sigma_{x2} = [(x-\ell)^2 + (y-y_o)^2 + z^2]^{1/2} \qquad \text{(A-15)}$$

and y_o is the distance between the line source and the x-axis as shown in Fig. 6.

The fluxes in the x and y directions are obtained by differentiation of Eq. (A-13) to give

$$-k\frac{\partial T}{\partial x}(x,y,z) = \frac{Q}{2\pi}\left\{\frac{1}{\sigma_{x2}} - \frac{1}{\sigma_{x1}}\right\} \qquad \text{(A-16)}$$

$$-k\frac{\partial T}{\partial y}(x,y,z) = \frac{Q}{2\pi}(y-y_o)\left\{\frac{1}{\sigma_{x2}(\sigma_{x2} + x - \ell)}\right.$$

$$\left. - \frac{1}{\sigma_{x1}(\sigma_{x1} + x + \ell)}\right\} \qquad \text{(A-17)}$$

If a similar line source is placed parallel to the y-axis and bisected by the x-axis, then the temperature rise is

$$T(x,y,z) = \frac{Q}{2\pi k} \ell n\left\{\frac{\sigma_{y1} + y + \ell}{\sigma_{y2} + y - \ell}\right\} \qquad \text{(A-18)}$$

where $\sigma_{y1} = [(x-x_o)^2 + (y+\ell)^2 + z^2]^{1/2}$ (A-19)

$$\sigma_{y2} = [(x-x_o)^2 + (y-\ell)^2 + z^2]^{1/2} \qquad \text{(A-20)}$$

and x_o is the distance between the line source and the y-axis.

The fluxes in the x and y directions are

$$-k\frac{\partial T}{\partial x}(x,y,z) = \frac{Q}{2\pi}(x-x_o)\left\{\frac{1}{\sigma_{y2}(\sigma_{y2} + y - \ell)}\right.$$

$$\left. - \frac{1}{\sigma_{y1}(\sigma_{y1} + y + \ell)}\right\} \qquad \text{(A-21)}$$

$$-k\frac{\partial T}{\partial y}(x,y,z) = \frac{Q}{2\pi}\left\{\frac{1}{\sigma_{y2}} - \frac{1}{\sigma_{y1}}\right\} \qquad \text{(A-22)}$$

Circular Ring Source Image

The potential due to a circular ring source of line strength Q and radius R on an adiabatic half-space is a classic problem of mathematical physics. The solution can be easily found in many references [6,7,8,13] and when expressed as a temperature rise the solution is

$$T(\rho,z) = \frac{2QR}{\pi k \sigma^{1/2}} K(\lambda) \qquad \text{(A-23)}$$

where $\sigma \equiv z^2 + (\rho+R)^2$ (A-24)

$$\lambda \equiv 2(\rho R/\sigma)^{1/2} \qquad \text{(A-25)}$$

and $K(\cdot)$ is the complete elliptic integral of the first kind. The polar coordinate system ρ-z has an origin at the centroid of the circular ring.

The radial flux can be obtained by differentiating Eq. (A-23) with respect to ρ to give

$$-k\frac{\partial T}{\partial \rho}(\rho,z) = \frac{2QR}{\pi}\left\{\frac{\rho+R}{\sigma^{3/2}} K(\lambda) + \frac{\sigma-\rho(2\rho+2R)}{2\sigma^{3/2}\rho}\right.$$

$$\left.[E(\lambda)/(1-\lambda^2) - K(\lambda)]\right\} \qquad \text{(A-26)}$$

where $E(\cdot)$ is the complete elliptic integral of the second kind.

The expression for the temperature rise due to a circular ring source can also be expressed as a series of Legendre polynomials similar to Eq. (A-7) for the circular contact with uniform flux [8]. However, the elliptic integral representation is more convenient because both complete elliptic integrals $E(\cdot)$ and $K(\cdot)$ can be calculated accurately, efficiently and simultaneously by the Gauss arithmetic-geometric mean process [14].

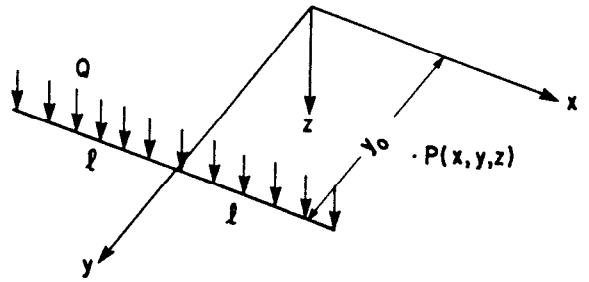

Fig. 6 Finite-line source on an adiabatic half-space